Effect of apoA-I PEGylation on the Biological Fate of Biomimetic High-Density Lipoproteins

Pedersbæk, Dennis; Krogager, Louise; Albertsen, Camilla Hald; Ringgaard, Lars; Hansen, Anders E.; Jønsson, Katrine; Larsen, Jannik B.; Kjær, Andreas; Andresen, Thomas L.; Simonsen, Jens B.

Published in:
ACS Omega

Link to article, DOI:
10.1021/acsomega.0c05468

Publication date:
2021

Document Version
Publisher's PDF, also known as Version of record

ACS OMEGA

http://pubs.acs.org/journal/acsodf

Article

Effect of apoA-I PEGylation on the Biological Fate of Biomimetic High-Density Lipoproteins

Dennis Pedersbæk, Louise Krogager, Camilla Hald Albertsen, Lars Ringgaard, Anders E. Hansen, Katrine Jønsson, Jannik B. Larsen, Andreas Kjær, Thomas L. Andresen, and Jens B. Simonsen*

Cite This: *ACS Omega* 2021, 6, 871−880

Read Online

ACCESS | Metrics & More | Article Recommendations | Supporting Information

ABSTRACT: Biomimetic high-density lipoproteins (b-HDL) have in the past two decades been applied for various drug delivery applications. As b-HDL inherently have relatively long circulation half-life and high tumor accumulation, this has inspired researchers to use b-HDL to selectively deliver drugs to tumors. PEGylation of the b-HDL has been pursued to increase the circulation half-life and therapeutic efficacy even further. The b-HDL consist of lipids stabilized by a protein/peptide scaffold, and while PEGylation of the scaffold has been shown to greatly increase the circulation half-life of the scaffold, the effect of PEGylation of the lipids is much less significant. Still, it remains to be evaluated how the biological fate, including cellular uptake, biodistribution, and circulation half-life, of the b-HDL lipids is affected by PEGylation of the b-HDL scaffold. We studied this with apolipoprotein A-I (apoA-I)-based b-HDL and mono-PEGylated b-HDL (PEG b-HDL) both *in vitro* and *in vivo*. We found that PEGylation of the b-HDL scaffold only seemed to have minimal effect on the biological fate of the lipids. Both b-HDL and PEG b-HDL overall shared similar biological fates, which includes cellular uptake through the scavenger receptor class B type 1 (SR-BI) and relatively high tumor accumulation. This highlights that b-HDL are dynamic particles, and the biological fates of the b-HDL components (lipids and scaffold) can differ. A phenomenon that may also apply for other multicomponent nanoparticles.

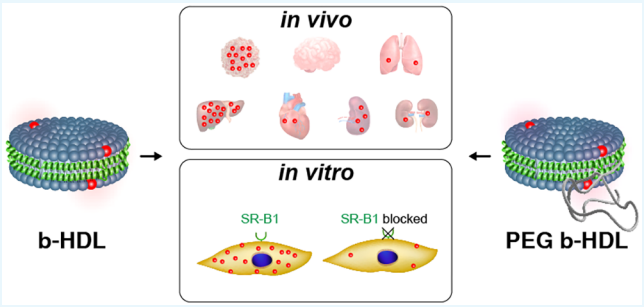

INTRODUCTION

Application of nanoparticles for drug delivery has in recent decades been the subject of much research interest due to the potential to significantly improve the therapeutic efficacy of drugs that are normally administered as free drugs.[1−3] However, it can be challenging to avoid clearance or agglomeration of the nanoparticles *in vivo*.[4] Surface grafting of polyethene glycol (PEG) to nanoparticles has been shown to be an effective strategy to overcome these challenges.[4−7] The hydrophilic PEG layer provides the nanoparticles with 'stealth'-like properties, which results in increased stability and circulation half-life of the nanoparticles.[4−6] The therapeutic potential of PEGylation is clearly illustrated by the several PEGylated drugs approved for clinical use.[4,5] This also includes the PEGylated liposomal formulation Doxil, which utilizes the long circulation half-life to increase the accumulation of drugs in the tumor by the enhanced permeability and retention (EPR) effect.[8]

A long circulation half-life can also be obtained with non-PEGylated nanoparticles.[9−11] One of these is the biomimetic high-density lipoproteins (b-HDL). The b-HDL are mimics of the endogenous high-density lipoproteins (HDL), which are 8−12 nm sized particles that play an important role in the metabolism of lipids in the body.[12,13] In particular, they are involved in the removal of excess cholesterol from the peripheral tissue to the liver for excretion as part of the reverse cholesterol transport.[12,14] The structure of HDL is dynamic, and it continuously changes as the HDL collect and deliver cholesterol, which involves remodeling by enzymes, HDL−lipid influx and efflux to and from cells, respectively, and lipid exchange with other lipoproteins. Overall, the HDL can be categorized as either discoidal with an apolipoprotein scaffold [typically, apolipoprotein A-I (apoA-I)] that stabilizes a lipid bilayer or spherical with a core primarily loaded with hydrophobic cholesterol ester and a surface comprising lipids and stabilizing apolipoprotiens.[14] Similarly, the types of b-HDL also vary greatly and include discoidal and spherical b-HDL that can be stabilized with either full-length apolipoproteins or mimicking peptides.[15] The various types of b-HDL are referred to by various nomenclatures, for example, reconstituted HDL typically refers to b-HDL prepared with full-length apoA-I,

Received: November 9, 2020
Accepted: December 8, 2020
Published: December 21, 2020

while synthetic HDL typically refers to b-HDL prepared with peptides. Although we in this study used discoidal b-HDL with apoA-I (Figure 1), we will use b-HDL as a generic term to refer to both this formulation and the other types of HDL-mimicking nanoparticles. Besides the relatively long circulation half-life (typically considered to be around 12−24 h,[13] but it is dependent on the specific b-HDL formulation[15]), the b-HDL possess several other properties that are advantageous in a drug delivery setting, including high biocompatibility, biodegradability, efficient penetration into tumors, and possible cellular uptake through endogenous receptors that normally recognize HDL and are overexpressed on many types of cancer cells.[12−14,16−18]

Despite the fact that the non-PEGylated b-HDL are considered to have relatively long circulation half-lives that are even comparable to those of PEGylated liposomes,[13,19] combining PEGylation and b-HDL has previously been pursued to increase their stability, circulation half-life, and the resulting therapeutic efficacy further.[20−22] PEG has been attached to either the lipids or the scaffold of the b-HDL. The studies using b-HDL with PEGylated lipids showed either no effect on the biological fate (using 16−21 nm b-HDL, spherical and stabilized with peptides)[11,19] or minor effects.[20,21] In particular, Li et al.[20] showed that PEGylation of the b-HDL lipids (approx. 10 nm b-HDL, discoidal and stabilized with peptides) can increase the circulation half-life of the lipids, depending on the amount of PEGylated lipids in the b-HDL and the length of the PEG chain. Furthermore, they showed no significant effect on the pharmacokinetics of the peptides by PEGylation of the lipids.[20] Tang et al.[21] showed that PEGylation of the b-HDL lipids (approx. 10 nm b-HDL, discoidal and stabilized with peptides) decreased the uptake of b-HDL in cells, but the biodistribution profile of their b-HDL was largely unaffected by the PEGylation, though the accumulation of PEGylated b-HDL in some organs seemed slightly decreased relative to non-PEGylated b-HDL. Instead of using PEGylated lipids, Murphy et al.[22] PEGylated apoA-I in discoidal b-HDL and showed up to sevenfold increased circulation half-life of the apoA-I scaffold as a result of the PEGylation. This is a much greater increase in the circulation half-life than reported in the studies using b-HDL with PEGylated lipids, which have reported up to 2.7-fold increase in the circulation half-life of the lipids by PEGylation with similar amounts of PEG.[20] Hence, it might be possible to affect the biological fate of the b-HDL lipids more significantly by PEGylation of the scaffold. A potentially longer circulation half-life of the b-HDL may lead to an enhanced therapeutic efficacy. For example, in the application of b-HDL for the treatment of atherosclerosis, this will likely increase the antiatherogenic activity of the b-HDL because of the extended period to remove excess cholesterol. Furthermore, in the application of b-HDL for targeting tumors, this will potentially reduce undesired uptake in nontargeted organs and cells and thus increase the accumulation in the tumor by the EPR effect.

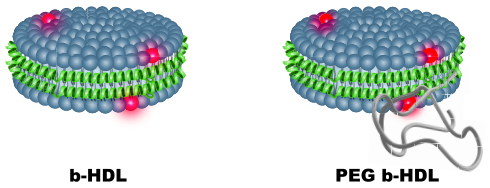

Figure 1. Illustrations of b-HDL (left) and PEG b-HDL (right) used in this study. They consist of lipids (blue), lipid-conjugated fluorophores (red), and an apoA-I scaffold (green). For PEG b-HDL, the PEG (gray) is conjugated to one of the two apoA-I scaffold proteins.

We have recently showed the importance of distinguishing between b-HDL lipids and the scaffold when assessing the biological fate of b-HDL.[15] However, most studies only track one component, for example, the studies using PEGylated lipids tracked the b-HDL by lipid labels, while Murphy et al.[22] PEGylated apoA-I and tracked the apoA-I scaffold. That said, we emphasize that the drugs used in b-HDL are often lipid-conjugated or hydrophobic; hence, the lipids can be considered as models of the drugs.[18,23]

In this study, we tried a yet unexplored approach for PEGylation and tracking of b-HDL, namely, PEGylation of the scaffold (Figure 1) and *in vitro* and *in vivo* evaluation of the effect on the biological fate of the lipids. We observed a slight decrease in the cellular uptake and slightly lower accumulation in some organs for PEG b-HDL compared to b-HDL. However, the cellular uptake and biodistribution of b-HDL and mono-PEGylated b-HDL (PEG b-HDL) were overall largely similar. Consequently, while mono-PEGylation of b-HDL can increase the circulation half-life of the apoA-I scaffold significantly,[22] it does not seem to have as pronounced an effect on the corresponding b-HDL lipids. This highlights the dynamic nature of the b-HDL, which has to be considered when the b-HDL are applied for drug delivery.

RESULTS AND DISCUSSION

Preparation of b-HDL and PEG b-HDL. The discoidal b-HDL were prepared with apoA-I by the detergent depletion method, as described elsewhere.[17,23] We used the phospholipid 1,2-dipalmitoyl-*sn*-glycero-3-phosphocholine (DPPC), 1 mol % of lipid-conjugated fluorophores [either 3,3′-dioctadecyloxacarbocyanine (DiO), 1,2-distearoyl-*sn*-glycero-3-phos- phoethanolamine-(Cyanine 5) (DSPE-Cy5), or 1,1′-dioctadecyl-3,3,3′,3′-tetramethylindotricarbocyanine iodide (DiR) that all should be stable incorporated into the b-HDL[23]], and apoA-I purified from human plasma.[23] Briefly, the lipids and apoA-I were mixed in a lipid/protein molar ratio of 100 in a solution containing detergent (20 mM cholate). The detergent was removed by incubation overnight with Bio-Beads to induce self-assembly of b-HDL. This yielded ∼10 nm-sized monodispersed particles, as determined by dynamic light scattering (DLS) and size-exclusion chromatography (SEC) using a Superose 6 Increase 10/300 GL column (Figure 2A). The assembled b-HDL were subsequently PEGylated with 20 kDa PEG on the apoA-I by mixing with amine-active functionalized PEG in a PEG:apoA-I ratio between 8 to 9. This should attach PEG to the primary amines of the apoA-I. The PEGylated b-HDL were hereafter applied to SEC (Figure 2B). Three major peaks appear in the SEC chromatogram. The peak close to 16 mL corresponds to the bare b-HDL, while the peak around 14 mL is expected to be the mono-PEGylated b-HDL. The peak around 12 mL, which has a clear shoulder towards lower retention volumes, likely corresponds to the poly-PEGylated b-HDL. Although the single PEG addition to the ∼170 kDa b-HDL only adds 20 kDa to the total molecular weight of the particle, the flexible PEG, behaving like a random coil, seemingly increases the specific molar volume and retention volume significantly.[24] This made it possible to separate b-HDL from the mono-PEGylated b-HDL (PEG b-HDL). The SEC analysis of the collected PEG b-HDL confirmed the

https://dx.doi.org/10.1021/acsomega.0c05468
ACS Omega 2021, 6, 871−880

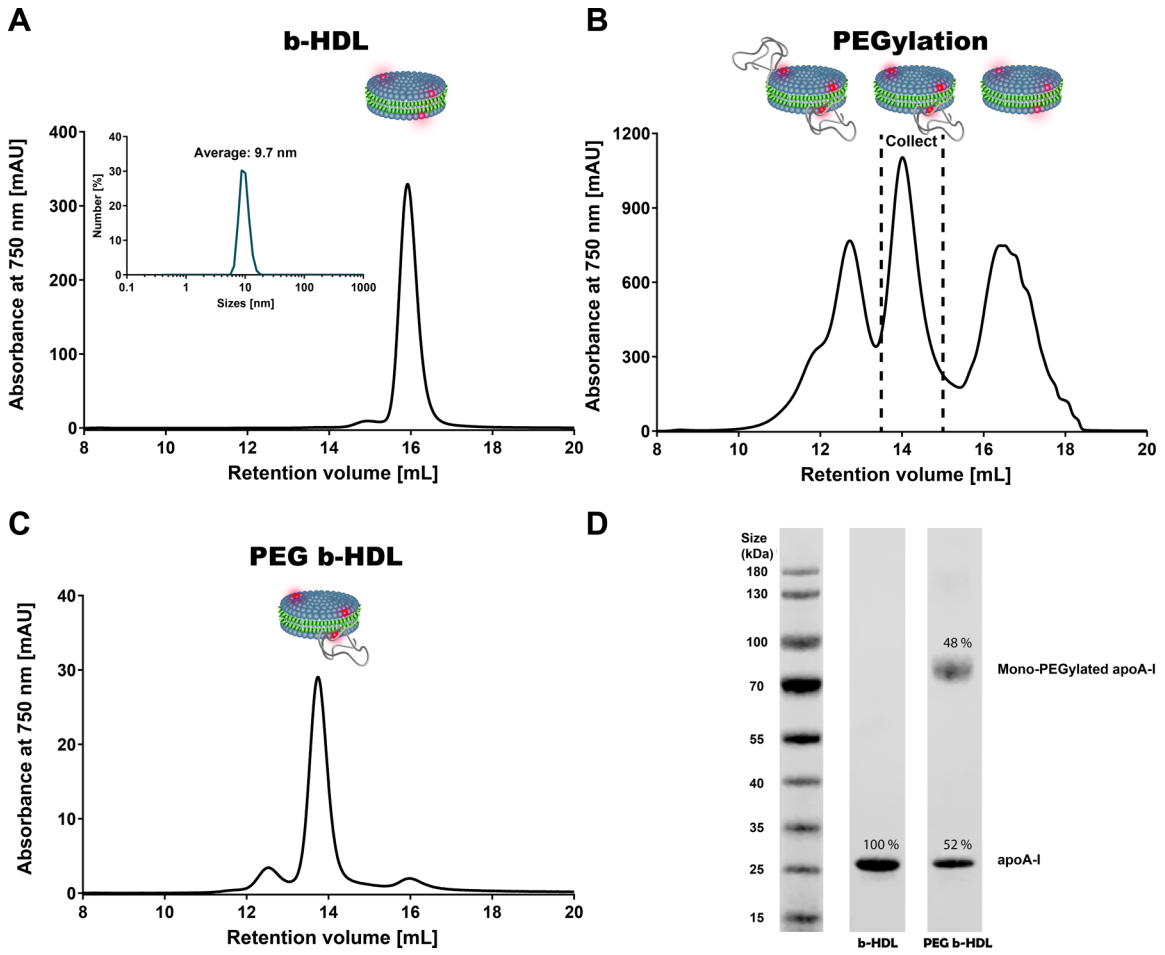

Figure 2. Characterization of b-HDL and the preparation of PEG b-HDL. (A) SEC characterization of the non-PEGylated b-HDL. A Superose 6 Increase 10/300 GL column was used, and absorbance from DiR at 750 nm was detected. DLS measurements are illustrated in the inset (the average size was estimated to be 9.7 nm). (B) SEC characterization of the b-HDL immediately after PEGylation. The peaks correspond to b-HDL with different degrees of PEGylation. The peak corresponding to the mono-PEGylated b-HDL (PEG b-HDL) was collected (13.5−15 mL). (C) Reanalyzing the collected PEG b-HDL showed that mono-PEGylated b-HDL were successfully isolated. (D) SDS-PAGE of b-HDL and PEG b-HDL.

successful isolation of stable and monodisperse PEG b-HDL (Figure 2C). As these discoidal b-HDL consist of two apoA-I proteins[12,25] (Figure 1), mono-PEGylation of b-HDL implies that approximately 50% of the apoA-I proteins are PEGylated. We confirmed that this was the case by SDS-PAGE (Figure 2D), which showed similar intensities of the apoA-I band (∼28 kDa) and mono-PEGylated apoA-I band (∼80 kDa). We also confirmed that poly-PEGylated b-HDL contained multi-PEGylated apoA-I (Figure S1). Notably, the increase in the size of PEGylated apoA-I relative to that of non-PEGylated apoA-I is estimated from the SDS-PAGE to be larger than the expected change by the addition of a 20 kDa PEG. A larger apparent size of PEGylated apoA-I on SDS-PAGE has also been shown before[22] and can be ascribed to aberrant migration because of the interactions between PEG and SDS, which is commonly seen for PEGylated proteins.[24] The successful preparation of both monodisperse b-HDL and PEG b-HDL with incorporated lipid-based fluorophores (probes for the lipids) allowed us to compare the biological fates of their lipids in the *in vitro* and *in vivo* experiments.

***In Vitro* Studies of the Cellular uptake of b-HDL and PEG b-HDL.** To determine whether the apoA-I PEGylation affected the cellular uptake of the b-HDL lipids, we used flow cytometry. We detected the lipid label DiO and compared the uptake of b-HDL and PEG b-HDL in the hepatocellular carcinoma cell line, HepG2 (see Figure S2 for the gating strategy). The HepG2 cells express the SR-BI receptor, which can mediate the uptake of the b-HDL cargo.[26] We found that both b-HDL and PEG b-HDL were taken up by the cells with a time-dependent uptake that steadily increased during the first 6 h (Figure 3A). The uptake of PEG b-HDL was only slightly lower than the uptake of b-HDL. The difference seemed most pronounced after 1 h, where it was estimated to be significant, but the difference was less distinct after 3 h and not significant after 6 h. A similar trend with decreasing difference between b-HDL and PEG b-HDL uptakes has also been shown by others, who used b-HDL with PEGylated lipids.[20] Furthermore, the time-dependent increase in the uptake of b-HDL and PEGylated b-HDL has also been observed by others.[20,21] We are aware that we cannot determine whether the b-HDL are internalized by the cells or simply adhere to their surface when we use conventional flow cytometry. Therefore, we used confocal microscopy to confirm that the lipid-conjugated fluorophores incorporated into the b-HDL were internalized (Figure 3B). We used a slice through the middle of the cell to assess the b-HDL internalization (Figure S3). We employed

https://dx.doi.org/10.1021/acsomega.0c05468
ACS Omega 2021, 6, 871−880

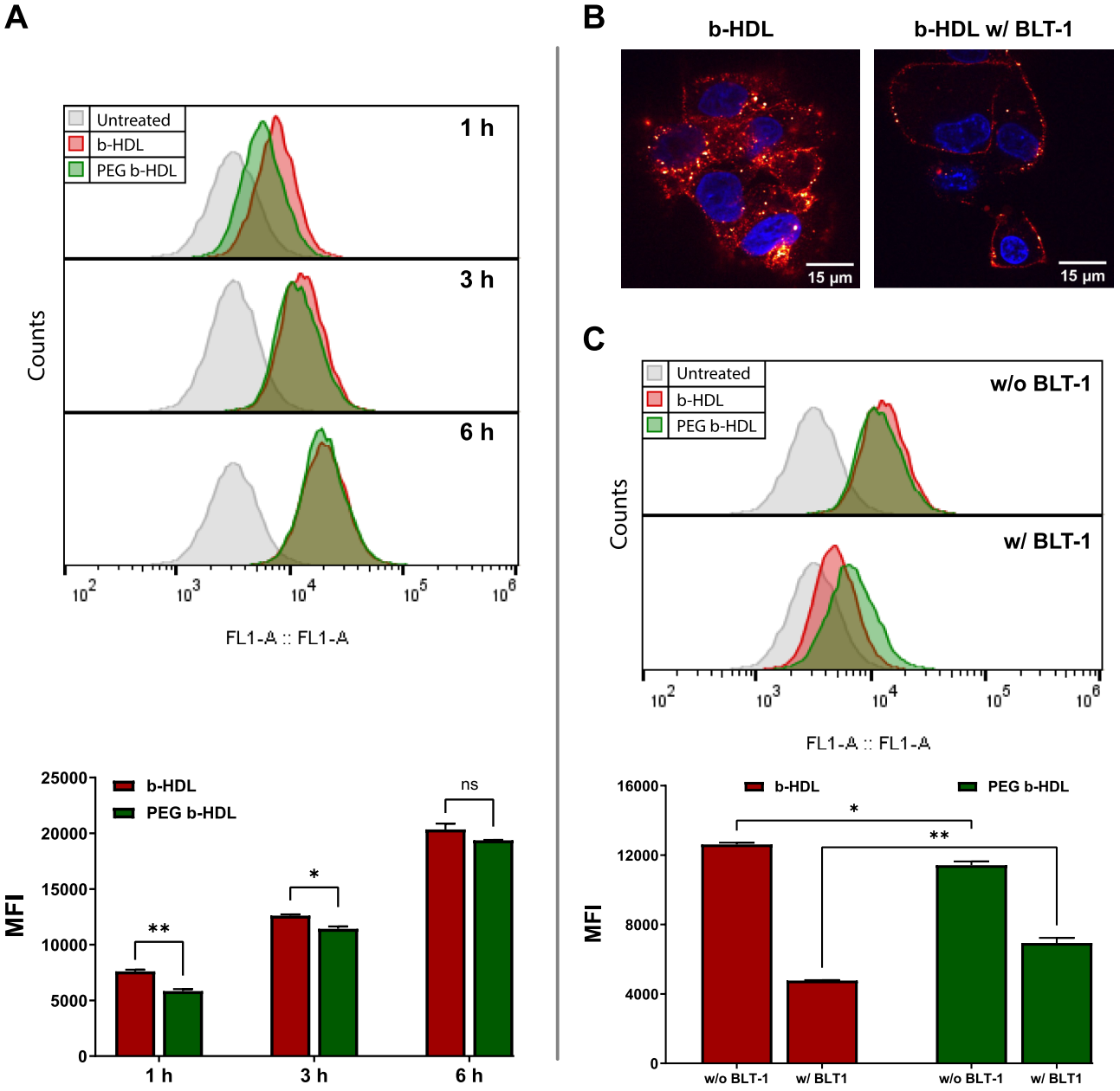

Figure 3. Uptake of b-HDL and PEG b-HDL in HepG2 cells. (A) Flow cytometry measurements, including histograms (top) and the median fluorescence intensity (MFI) (bottom), measured after the cells had been incubated for 1, 3, or 6 h with b-HDL/PEG b-HDL. The incorporated DiO label was detected. (B) Confocal microscopy of the b-HDL uptake studied after 1.5 h of incubation with b-HDL. The b-HDL were labeled with DSPE-Cy5 (red), and the nuclei were stained with DAPI (blue). To assess the internalization, we studied a slice through the middle of the cells. The b-HDL were internalized in the HepG2 cells (left); however, the internalization was greatly diminished after blocking SR-BI with BLT-1 (right). (C) Flow cytometry measurements, including histograms (top) and MFI (bottom), measured after 3 h of incubation with HepG2 cells, either with or without pretreatment for 1 h with 100 μL BLT-1. The MFI data represent mean ± SEM (n = 2−3). Statistical comparisons were conducted with a two-way ANOVA, *, $p \leq 0.05$, **, $p < 0.01$.

the small-molecule SR-BI blocker, Block Lipid Transport-1 (BLT-1),[27] to evaluate whether the internalization depended on the SR-BI receptor. The b-HDL fluorescence signal inside the cells, close to the nuclei, indicates b-HDL internalization, which is diminished after blocking SR-BI (Figure 3B). This suggests that the b-HDL lipids are internalized by a SR-BI-dependent uptake mechanism. Whereas these microscopy data remain qualitative, other methods, e.g., imaging flow cytometry, could be used to evaluate the internalization quantitatively.[17] However, the data strongly support that the b-HDL association with the cells measured by the flow cytometry (Figure 3A,C) corresponds to the cellular uptake.

To compare the SR-BI dependence of the uptake of the b-HDL and PEG b-HDL in a high-throughput manner, we performed flow cytometry measurements using HepG2 cells both with and without pretreatment with BLT-1. The BLT-1-treated cells were incubated with 100 μM BLT-1 for 1 h before applying b-HDL for 3 h. It is evident that the BLT-1 decreased the uptake of both b-HDL and PEG b-HDL (Figure 3C), which confirms the importance of SR-BI. As BLT-1 blocks lipid transport through SR-BI,[27] this indicates decreased

https://dx.doi.org/10.1021/acsomega.0c05468
ACS Omega 2021, 6, 871−880

internalization of b-HDL lipids. Apparently, both the b-HDL and PEG b-HDL lipids were also to some extent taken up by a SR-BI-independent mechanism, which could also include b-HDL/PEG b-HDL bound to the membrane, for example, by BLT-1-blocked SR-BI that can bind b-HDL/PEG b-HDL but not internalize their lipid cargo. The uptake after BLT-1 treatment seems slightly higher for PEG b-HDL than for b-HDL ($p < 0.01$). Although the difference is minor, this could indicate an alternative SR-BI-independent mechanism more specific for PEG b-HDL than for b-HDL. Nonetheless, it is notable that the uptake of PEG b-HDL is partly SR-BI-dependent. One could have imagined that the PEG attached on apoA-I would shield the interactions with SR-BI as apoA-I is known to facilitate interactions with SR-BI.[28] However, the attachment of a single PEG on apoA-I might not be sufficient to shield the interactions with SR-BI. This would also be consistent with the results from Murphy et al.,[22] who showed preserved cholesterol mobility of mono-PEGylated b-HDL, thereby indicating preserved receptor-mediated interactions with the PEGylated b-HDL. Alternatively, the minimal effects of PEGylation might be because the b-HDL were remodeled and the lipids, including the lipid labels, were exchanged to other lipoproteins present in the serum. Such remodulations are inherent features of HDL,[29−31] and we have recently shown that lipid desorption and b-HDL remodeling can occur without enzyme activity, but *via* direct interaction with the endogenous lipoproteins.[23] The desorption of lipid labels from the b-HDL could potentially result in uptake of the lipid labels independent of the b-HDL particle; however, we used lipid-conjugated fluorophores that should exhibit minimal fluorophore desorption in biological environments.[23] Despite the fact that we only observed minor effects from PEGylation in the *in vitro* setting, the effects might be more pronounced *in vivo*, where the slight shielding from cellular uptake caused by PEGylation might be sufficient to alter the biological fate, including biodistribution and circulation half-life of the b-HDL.

***In Vivo* Biodistribution Studies of b-HDL and PEG b-HDL.** To determine the effect of PEGylation of apoA-I on the biological fate of the b-HDL lipids *in vivo*, we investigated the biodistribution and pharmacokinetics in 9−10 weeks old female BALB/c mice with established CT26 tumors on the right flank (a syngeneic mouse model). Importantly, the CT26 cells express SR-BI,[32] but SR-BI is also expressed in several other organs, in particular on the cells in the liver.[12] The b-HDL were injected intravenously (tail vein) using a dose of 3 mg apoA-I/kg. Both the b-HDL and PEG b-HDL were labeled with the near-infrared fluorophore DiR, and the mice were imaged with an IVIS Lumina XR (PerkinElmer) at multiple time points (Figure 4A,B). Evidently, both the b-HDL and PEG b-HDL lipids gradually accumulated in the tumor. However, it is difficult to assess the relative distribution between the organs from the whole-body images. Hence, the organs were harvested after 48 h, imaged (Figure 4A,B), and the fluorescence intensities of the whole organs were quantified using Living Image software (Figure 4C). From these measurements, we observe a relatively high tumor accumulation of both b-HDL and PEG b-HDL lipids compared to what has been reported for other commonly used tumor-targeting nanoparticles, e.g., liposomes, polymeric nanoparticles, etc.[33−35] The PEG b-HDL displayed a slightly lower tumor accumulation than b-HDL ($p < 0.05$). A lower accumulation of PEG b-HDL relative to b-HDL is also observed in the liver and lungs, although less pronounced than in the tumor. While it could have been speculated that PEGylation of b-HDL would result in increased accumulation in the tumor due to an extended circulation half-life and the EPR effect, this does not seem to be the case. Rather, the slightly lower accumulation of PEG b-HDL lipids in some organs is comparable to the effects obtained by PEGylation of the b-HDL lipids, as evaluated by Tang et al.[21] The similar biodistribution of the lipids in b-HDL with PEG on either the scaffold or lipids supports the notion that b-HDL lipids do not follow the same biodistribution as the scaffold. We speculate that either the lipids are delivered to the cells without uptake of apoA-I or the b-HDL are remodeled, and the lipids are exchanged to the endogenous lipoproteins. As estimated from the *in vitro* experiments (Figure 3) the cellular uptake of b-HDL lipids can be slightly affected by the presence of PEG. Similarly, the b-HDL remodeling and lipid exchange might also be affected by PEG. This could explain the minor differences between the b-HDL and PEG b-HDL biodistribution.

Although *ex vivo* measurements on the harvested organs are widely used to assess the biodistribution of b-HDL,[21,36−38] and that we have used them for comparison of b-HDL and PEG b-HDL, they cannot be considered as accurate quantitative measurements of the biodistribution. Quantification of the fluorescence signal from the organs is limited due to scattering of the emitted photons from the organs and possible quenching effects caused by high fluorophore concentration and/or interactions with its local environment.[39] Hence, we homogenized the organs and quantified the fluorescence signal in the homogenates (Figure 4D). We ensured that the effects from quenching were limited, as the measurements were conducted in the range where the fluorescence increased linearly with concentration (Figure S4). We used a DiR standard curve (Figure S5) and weight of the organs (Table S1) to obtain the injected dose, % injected dose (ID)/g. Evidently, the biodistribution obtained from the homogenates looks somewhat different than the biodistribution obtained from the whole organs *ex vivo*, as the highest accumulation of b-HDL is now determined to be in the liver. This could be explained by the larger size of the liver, which likely caused a lower fluorescence signal before homogenization because of increased tissue absorbance relative to the other organs. Moreover, the measured accumulation in the spleen also differs between the two methods used to quantify the biodistribution. This might be due to the fact that the spleen contains much blood,[40] which could have affected the fluorescence from the whole organ. The environment around the fluorophores was similar after homogenization, which allowed for a more quantitative comparison of the signal from the organs. The greater accumulation of b-HDL lipids in the liver relative to that in the tumor has also been shown by others with more quantitative radioactive methods.[11,41] Furthermore, we have recently conducted a comprehensive systematic review of the biodistribution of several types of b-HDL,[15] and the biodistribution estimated from the homogenates corresponds well with the expected biodistribution of the b-HDL from our systematic review. This highlights the importance of homogenization for a more quantitative assessment of the biodistribution when using fluorescence readout.

From the biodistribution determined from the homogenates, we again observe a slightly lower accumulation of PEG b-HDL lipids in the tumor relative to that of b-HDL ($p < 0.05$). If the circulation half-life of PEG b-HDL was much longer than that

https://dx.doi.org/10.1021/acsomega.0c05468
ACS Omega 2021, 6, 871−880

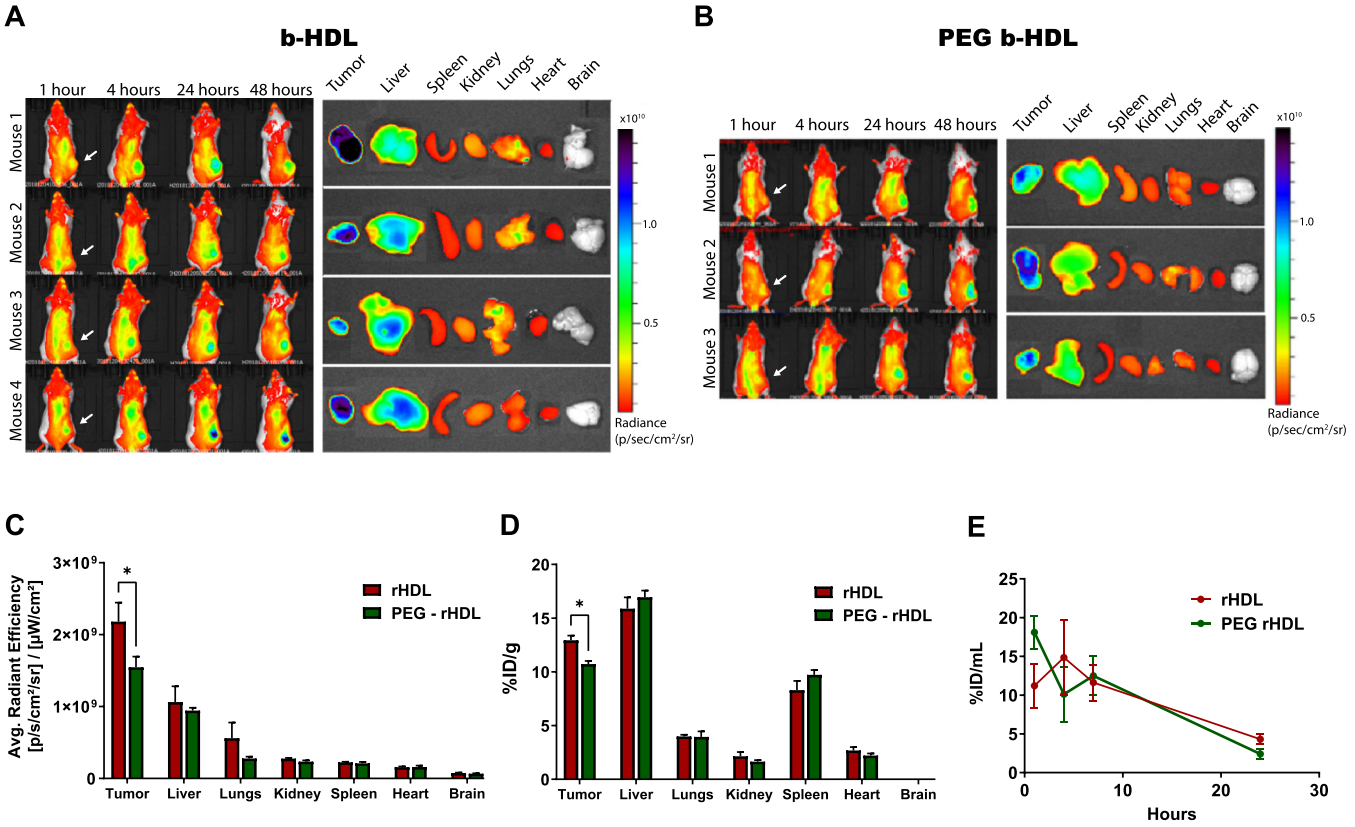

Figure 4. Evaluation of how apoA-I PEGylation affects the biological fate of b-HDL lipids *in vivo* using BALB/c mice with a CT26 tumor. The b-HDL were labeled with the near-infrared fluorophore DiR. Whole-body images and harvested organs for b-HDL (A) and PEG b-HDL (B). The white arrows in the first time point indicate the position of the tumor. (C) Biodistribution estimated from fluorescence of the whole organs *ex vivo*. (D) Biodistribution estimated from fluorescence of homogenized organs. (E) Pharmacokinetics of the b-HDL and PEG b-HDL estimated from three mice in each group. Three samples were drawn from each mouse, one at the first time point (1 h) and then distributed between the remaining time points (4, 7, and 24 h) so that each point is based on a minimum of two measurements. Data in (C−E) represent mean ± SEM (n = 3−4 in (C−D) and n = 2−3 in E). Statistical comparisons were conducted with a two-way ANOVA, *, $p < 0.05$.

of b-HDL, more PEG b-HDL might be present in the circulation, which could explain this difference. However, estimation of the pharmacokinetics of b-HDL and PEG b-HDL showed no apparent difference (Figure 4E). We emphasize that these measurements were conducted tracking the lipid label, and the biodistribution and pharmacokinetics of apoA-I are expectedly affected more significantly by the modification with PEG, as shown by Murphy et al.[22]

Overall, the differences between the biological fate of b-HDL and PEG b-HDL lipids both *in vitro* and *in vivo* are minimal. The effects might be more pronounced if more PEG were conjugated to the b-HDL; however, multi-PEGylation might also interfere with the stability of the b-HDL. We, therefore, used an amount of PEG in the b-HDL (20 kDa PEG per b-HDL) similar to the amount used in other studies.[11,20−22] The minimal effect on the fate of the b-HDL lipids caused by PEGylation of the scaffold stand in marked contrast to the sevenfold increase in the circulation half-life of the apoA-I after apoA-I PEGylation observed by Murphy et al.,[22] but it does resemble the effect on the biological fate of the b-HDL lipids reported to be caused by PEGylation of b-HDL lipids.[11,20,21] This indicates that the b-HDL lipids do not share the same biological fate as the apoA-I scaffold. Notably, this is also the case for endogenous HDL. The HDL lipids can be delivered to cells without uptake of apoA-I, which subsequently can take up lipids to form new HDL particles. Similar principles likely apply for the apoA-I and PEGylated apoA-I initially associated to the b-HDL, which may be reused *in vivo* to form new HDL particles with endogenous lipids, after they have delivered their initial lipid cargo. The larger size of PEGylated apoA-I relative to that of non-PEGylated apoA-I may affect its clearance, for example, accumulation in the kidney requires passage through filtration barriers[42] that may limit the passage of the larger PEGylated apoA-I. This could explain the longer circulation half-life of PEGylated apoA-I relative to that of apoA-I.[22] Furthermore, as it is the case for endogenous HDL, the b-HDL lipids, including lipid labels, are likely also exchanged to other endogenous lipoproteins. Taken together, this stresses the dynamic nature of the b-HDL and the important distinction between the scaffold and lipid components of b-HDL. Though the b-HDL components inherently have different biological fates, other multicomponent drug delivery particles may also experience different fates of the individual components *in vivo*. For example, different types of lipids in the lipid bilayer of liposomes can have different propensity to desorb from the liposomes.[43] Hence, awareness of this phenomenon is important for the design of many types of drug delivery systems.

CONCLUSIONS

We have investigated the effects of apoA-I PEGylation on the biological fate of the lipids in discoidal b-HDL, which we evaluated both *in vitro* and *in vivo*. Fluorescence measurements of both whole and homogenized organs revealed that the b-

https://dx.doi.org/10.1021/acsomega.0c05468
ACS Omega 2021, 6, 871−880

HDL and PEG b-HDL lipids accumulated well in the tumor tissue. The measurements on the whole organs and homogenized organs showed some differences, but the results from the homogenized organs correspond well with the expected b-HDL biodistribution. Although significant effects of apoA-I PEGylation have been reported for the apoA-I associated to b-HDL, our findings indicate that the biological fate of b-HDL lipids is only minimally affected by PEGylation of the scaffold. Hence, whereas apoA-I PEGylation can be used as a tool to increase the circulation half-life of apoA-I, it does not seem to affect the biological fate of the b-HDL lipids, which likely is more dependent on the b-HDL dynamics, remodeling, and interactions with cells and endogenous lipoproteins. In this context, a potential slight gain in therapeutic efficacy obtained by using PEGylated b-HDL must be considered along with potential toxicities associated to *anti*-PEG immunity.[44] Overall, our study supports the notion that b-HDL can be used to deliver therapeutics to tumors. Furthermore, it highlights how thorough consideration of each component of nanoparticles for drug delivery must be employed, as there might be more complex dynamics *in vivo* that can cause a varying biological fate of the individual components.

EXPERIMENTAL SECTION

Materials. DPPC was supplied by Avanti Polar Lipids (USA), while the fluorophores DiO, DSPE-Cy5, and DiR were supplied by ThermoFisher Scientific (USA). PEG-ALD-20K and PEG-NHS-20K were both supplied by JenKem Technology. Phosphate buffered saline (PBS), fetal bovine serum (FBS), penicillin and streptomycin (PS), sodium cholate hydrate, NaCl, sodium acetate, and sodium cyanoborohydride, Trizma hydrochloride (Tris), trypsin, ethylenediaminetetraacetate (EDTA), sample buffer Laemmli 2× for SDS-PAGE, and BLT-1 were all supplied by Sigma-Aldrich (Denmark). Glycerol(UltraPure Glycerol) was supplied by Invitrogen, and minimum essential media (MEM), Dulbecco's modified Eagle medium (DMEM), SimplyBlue SafeStain, running buffer (NuPAGE MOPS SDS), protein ladder (PageRuler, prestained), NuPAGE Novex 4−12% bis-tris SDS gel, DAPI (4′,6-diamidino-2-phenylindole, dihydrochloride), NP-40 Surfact-Amps detergent solution, and Halt protease and phosphatase single-use inhibitor cocktail (100×) were supplied by ThermoFisher Scientific (USA).

Preparation and Characterization of b-HDL and PEG b-HDL. *b-HDL Preparation.* The discoidal b-HDL were prepared with full-length apoA-I using the detergent depletion method. The apoA-I (purity > 99%) was isolated from the human plasma, as described elsewhere.[23] Initially, the lipids (99 mol % DPPC and 1 mol % of either DiO, DSPE-Cy5, or DiR) were mixed in a 9:1 *tert*-butanol:MillQ solution and subsequently freeze-dried. The lipids were rehydrated in PBS with 20 mM sodium cholate and apoA-I, yielding a 5−7 mM total lipid concentration and lipid/protein ratio of 100. The sodium cholate was removed by incubation overnight with 0.6 μg Bio-Beads (Bio-Rad, Denmark) per μL at 41 °C. The solution was separated from the Bio-Beads by perforating a hole in the 2 mL Eppendorf tube and gently spinning it into a 15 mL Falcon tube. The b-HDL were characterized by both DLS using a ZetaSizer Nano ZS from Malvern Instruments and SEC using a Superose 6 Increase 10/300 GL column (GE Healthcare) equipped on a high-performance liquid chromatography system from Shimadzu (a LC-20AD pump, a DGU-20A SR degassing unit, a SIL-20AC HT autosampler, a SPD-M20A photodiode array detector, and a FRC-10A fraction collector).

b-HDL PEGylation. PEGylation of b-HDL was conducted on the assembled b-HDL using aldehyde PEGylation or NHS PEGylation for the *in vitro* and *in vivo* studies, respectively. Two different PEGylation strategies were employed as the DiR fluorophore required for the *in vivo* experiments was not compatible with the reduction step during the aldehyde PEGylation. Importantly, the outcome of the two different PEGylation strategies was similar (Figure S6). For the aldehyde PEGylation, the b-HDL solution was first exchanged by dialysis to a 20 mM sodium acetate buffer (pH 5.5). The solution was then mixed with 0.4 mM PEG-ALD-20K (dissolved in 50 mM sodium acetate) to yield an apoA-I:PEG-ALD-20K ratio of approx. 9. After 30 min, 10 mM sodium cyanoborohydride (dissolved in 50 mM sodium acetate) was added. The reaction was conducted overnight at 4 °C (in fumehood) using a MultiTherm shaker with heating and cooling (Benchmark Scientific). The reaction was quenched by the addition of 1 M Tris to yield a 0.1 M Tris concentration in the solution, before applying it to SEC where the mono-PEGylated b-HDL were collected. For the NHS PEGylation, the b-HDL was mixed in PBS with 8 M excess of NHS-PEG (20 kDa). The reaction was conducted at room temperature for 2 h, before the b-HDL/PEGylated b-HDL were concentrated (using a 30 MWCO spin filter). The solution was immediately hereafter loaded on SEC to remove the NHS-PEG and thereby stop the reaction. The mono-PEGylated b-HDL were collected.

Sodium Dodecyl Sulfate-PolyAcrylamide Gel Electrophoresis. The b-HDL and PEG b-HDL were also characterized by sodium dodecyl sulfate (SDS)-PAGE. Briefly, the samples were diluted in the SDS sample buffer 1:1 and heated to 80 °C for 10 min, before being added to the gel (4−12% Bis-Tris SDS gel) in the XCell SureLock Mini-Cell electrophoresis system (Thermo Fisher Scientific) loaded with 800 mL of the running buffer. The protein ladder (PageRuler Prestained) was used as the ladder. The gel was run for approximately 75 min using 150 V. Hereafter, the gel was washed and stained with SimplyBlue SafeStain for 1 h. The gel was destained in demineralized water overnight with a change of the demineralized water after 1 h. The gel was imaged with Li-Cor Odyssey FC.

***In Vitro* Evaluation of the uptake in HepG2 Cells.** *Cell Culture.* The HepG2 cells were cultured in MEM supplemented with 10% FBS and 1% PS.

Flow Cytometry. Prior to the flow cytometry measurements, 4×10^5 cells were seeded in a 48-well cell culture plate (ThermoFisher Scientific) at a volume of 250 μL per well and cultured for 24 h (37 °C, 5% CO_2). For the BLT-1-treated cells, 100 μM BLT-1 (diluted in medium) was added (100 μL) and incubated for 1 h before adding the particles. To add the b-HDL/PEG b-HDL, the media were first aspirated from the wells, and b-HDL/PEG b-HDL dissolved in media were added at a concentration of 50 μg apoA-I/mL at a volume of 200 μL (the apoA-I concentration was estimated by absorbance at 280 nm, measured by a NanoDrop 2000/2000c spectrophotometer (Thermo Fisher Scientific)). After incubation for the relevant period (1−6 h), the media were aspirated from the wells, and the cells were washed twice with 800 μL PBS. Then, 250 μL of trypsin solution (0.05% v/v trypsin and 0.53 mM EDTA) was added and incubated with the cells until cell detachment

https://dx.doi.org/10.1021/acsomega.0c05468
ACS Omega 2021, 6, 871−880

(approx. 5 min). Next, 800 μL of media was added to inactivate trypsin, and the cell suspensions were transferred to 2 mL Eppendorf tubes. The cell suspensions were centrifuged (200 g, 3 min, 20 °C), the supernatant was removed, and the cell pellet was resuspended in PBS and analyzed using flow cytometry, counting 10,000 cells in each sample. The gating strategy is presented in Figure S2.

Confocal Microscopy. For the confocal microscopy experiments, we incubated 20,000 HepG2 cells overnight in an ibidi μ-slide glass bottom chamber (cat. no. 80827) containing 300 μL of the medium (DMEM). The cells were then switched to fresh medium either with or without BLT-1 (100 μM) and incubated for 1 h, before the DSPE-Cy5-labeled b-HDL were added using 20× dilution of the b-HDL stock that had been prepared with a 2.5 mM lipid concentration. The cells were incubated for 1.5 h with the b-HDL (containing 1 mol % DSPE-Cy5). Then, the cells were fixed by adding 4% paraformaldehyde in PBS for 15 min at room temperature, before the cells were washed three times in PBS. Next, the cells were labeled with 5 μg/mL DAPI (diluted in PBS) by incubation for 5 min, following washing in PBS (three times). Hereafter, the cells were imaged using a Nikon Ti2, Yokogawa CSU-W1 spinning disc confocal microscope equipped with a 60x oil immersion, CFI Plan Apochromat Lambda NA 1.4 objective, and a Photometrics Prime 95B sCMOS detector. DAPI was excited by a 405 nm laser and detected through a 442/42 BrightLine HC bandpass filter, while DSPE-Cy5 was excited by a 488 nm laser and detected through a 700/75 ET bandpass filter.

***In Vivo* Evaluation of biodistribution and Pharmacokinetics.** *Biodistribution.* Seven 9−10 week-old female BALB/c mice were inoculated with 3×10^5 CT26 cells in the right flank 2 weeks prior to injection with b-HDL (four mice) or PEG b-HDL (three mice) at a dose of 3 mg apoA-I/kg (the apoA-I concentration was estimated by absorbance at 280 nm). Whole-body fluorescence images of the mice (anaesthetized with isoflurane before and during scanning) were conducted at 1, 4, 24, and 48 h post injection by detection of the DiR label using an IVIS Lumina XR (PerkinElmer). Two control mice confirmed that there was no detectable background signal. After 48 h, the mice were sacrificed (by cervical dislocation), and the tumor, liver, spleen, kidney, lungs, heart, and brain were harvested. The organs were imaged *ex vivo* with the IVIS Lumina XR, and the images were analyzed in Living Image software to obtain the average radiant efficiency for each organ. Subsequently, the harvested organs were homogenized using either Covaris automated dry homogenizer or a Precellys 24 three-dimensional bead-beating instrument. For the Covaris automated dry homogenizer, the organs were frozen in liquid nitrogen, before being smashed. The tissue powder obtained after smashing the organs was resuspended in the lysis buffer containing 50 mM Tris, 150 mM NaCl, 10% Glycerol, 1% NP-40 (pH 7.5), and 10 μL/mL of freshly added protease and phosphatase inhibitor cocktail. For the Precellys 24, the organs were added to 900 μL of lysis buffer, before they were added to the instrument in disposable tubes prefilled with ceramic beads of zirconium oxide, and homogenized (using 6500 rpm three times for 20 s with 5 min cooling in between). For both homogenization methods, the final concentration of the homogenate was 0.066 g/mL. After homogenization, the solutions with homogenized organs were incubated for 1 h at 4 °C and hereafter centrifuged (10,000 rpm, 15 min), and the supernatant was collected. The fluorescence of the homogenized organs was quantified using a TECAN Spark microplate reader (TECAN) using excitation and emission wavelengths of 750 and 785 nm, respectively, both with a bandwidth of 10 nm. Using standard curves of DiR (Figure S5) and the known tissue weight (Table S1), it was possible to obtain the biodistribution in %ID/g.

Pharmacokinetics. To investigate the pharmacokinetics, blood was drawn from the CT26 tumor-bearing mice injected with b-HDL (three mice) and PEG b-HDL (three mice) at a dose of 3 mg apoA-I/kg. Three blood samples were drawn from each mouse, one at the first time point (1 h), while the other samplings were distributed between the other time points (4, 7, an 24 h), such that the data from each time point is based on minimum two measurements. The blood (10−30 μL) was drawn from the facial vein and collected in PCR tubes prefilled with 10 μL of EDTA and saline water (1 μL 0.5 M EDTA with 9 μL saline water). The tubes were weighted before and after the collection of the blood to determine the weight of the blood. The volume of the blood was estimated by using the density of whole blood, which we assumed to be 1.06 g/mL. To lyse blood cells, 15 μL/mg lysis buffer was added to the whole blood. The samples were centrifuged at 10,000 rpm, and the supernatants were collected for fluorescence measurements, which were conducted similarly to the measurements on the homogenized organs. Using the standard curve of DiR (Figure S5) and the estimated blood volume, the %ID/mL could be obtained.

■ ASSOCIATED CONTENT

Supporting Information

The Supporting Information is available free of charge at https://pubs.acs.org/doi/10.1021/acsomega.0c05468.

SDS-page of PEGylated b-HDL with different degrees of PEGylation; illustration of the flow cytometry gating strategy; SDS-page of PEGylated b-HDL with different degrees of PEGylation; supporting confocal microscopy images; fluorescence measurements of the tissue homogenates at different concentrations for b-HDL; DiR standard curves used for the *in vivo* experiments; SEC analysis of b-HDL after aldehyde PEGylation; and weight of the harvested organs (PDF)

■ AUTHOR INFORMATION

Corresponding Author

Jens B. Simonsen − *Department of Health Technology, Biotherapeutic Engineering and Drug Targeting, Technical University of Denmark, 2800 Kongens Lyngby, Denmark;* orcid.org/0000-0002-4797-8570; Email: jbak@dtu.dk

Authors

Dennis Pedersbæk − *Department of Health Technology, Biotherapeutic Engineering and Drug Targeting, Technical University of Denmark, 2800 Kongens Lyngby, Denmark;* orcid.org/0000-0001-8900-8954

Louise Krogager − *Department of Health Technology, Biotherapeutic Engineering and Drug Targeting, Technical University of Denmark, 2800 Kongens Lyngby, Denmark*

Camilla Hald Albertsen − *Department of Health Technology, Biotherapeutic Engineering and Drug Targeting, Technical University of Denmark, 2800 Kongens Lyngby, Denmark*

https://dx.doi.org/10.1021/acsomega.0c05468
ACS Omega 2021, 6, 871−880

Lars Ringgaard − *Department of Health Technology, Biotherapeutic Engineering and Drug Targeting, Technical University of Denmark, 2800 Kongens Lyngby, Denmark*
Anders E. Hansen − *Department of Health Technology, Biotherapeutic Engineering and Drug Targeting, Technical University of Denmark, 2800 Kongens Lyngby, Denmark*
Katrine Jønsson − *Department of Health Technology, Biotherapeutic Engineering and Drug Targeting, Technical University of Denmark, 2800 Kongens Lyngby, Denmark*
Jannik B. Larsen − *Department of Health Technology, Biotherapeutic Engineering and Drug Targeting, Technical University of Denmark, 2800 Kongens Lyngby, Denmark*
Andreas Kjær − *Department of Clinical Physiology, Nuclear Medicine and PET and Cluster for Molecular Imaging, Department of Biomedical Sciences, Rigshospitalet and University of Copenhagen, 2100 Copenhagen, Denmark;* orcid.org/0000-0002-2706-5547
Thomas L. Andresen − *Department of Health Technology, Biotherapeutic Engineering and Drug Targeting, Technical University of Denmark, 2800 Kongens Lyngby, Denmark*

Complete contact information is available at: https://pubs.acs.org/10.1021/acsomega.0c05468

Notes

The authors declare no competing financial interest.

■ ACKNOWLEDGMENTS

The authors thank Camilla Stavnsbjerg for assistance with organ homogenization, Niklas Petersen and Jacob Bodekær Rasmussen for work on the optimization of the apoA-I PEGylation protocol, Nayere Taebnia for assistance with the TOC graphic, and Nicolai Paulsen for language-focused proof reading.

■ REFERENCES

(1) Allen, T. M.; Cullis, P. R. Drug Delivery Systems: Entering the Mainstream. *Science* **2004**, *303*, 1818−1822.
(2) Patra, J. K.; Das, G.; Fraceto, L. F.; Campos, E. V. R.; Rodriguez-Torres, M. D. P.; Acosta-Torres, L. S.; Diaz-Torres, L. A.; Grillo, R.; Swamy, M. K.; Sharma, S.; Habtemariam, S.; Shin, H.-S. Nano based drug delivery systems: recent developments and future prospects. *J. Nanobiotechnol.* **2018**, *16*, 71.
(3) Yu, X.; Trase, I.; Ren, M.; Duval, K.; Guo, X.; Chen, Z. Design of Nanoparticle-Based Carriers for Targeted Drug Delivery. *J. Nanomater.* **2016**, *2016*, 1−15.
(4) Hussain, Z.; Khan, S.; Imran, M.; Sohail, M.; Shah, S. W. A.; de Matas, M. PEGylation: a promising strategy to overcome challenges to cancer-targeted nanomedicines: a review of challenges to clinical transition and promising resolution. *Drug Delivery Transl. Res.* **2019**, *9*, 721−734.
(5) Jokerst, J. V.; Lobovkina, T.; Zare, R. N.; Gambhir, S. S. Nanoparticle PEGylation for imaging and therapy. *Nanomedicine* **2011**, *6*, 715−728.
(6) Mishra, P.; Nayak, B.; Dey, R. K. PEGylation in anti-cancer therapy: An overview. *Asian J. Pharm. Sci.* **2016**, *11*, 337−348.
(7) Suk, J. S.; Xu, Q.; Kim, N.; Hanes, J.; Ensign, L. M. PEGylation as a strategy for improving nanoparticle-based drug and gene delivery. *Adv. Drug Delivery Rev.* **2016**, *99*, 28−51.
(8) Barenholz, Y. Doxil® - The first FDA-approved nano-drug: Lessons learned. *J. Controlled Release* **2012**, *160*, 117−134.
(9) Peng, S.; Ouyang, B.; Men, Y.; Du, Y.; Cao, Y.; Xie, R.; Pang, Z.; Shen, S.; Yang, W. Biodegradable zwitterionic polymer membrane coating endowing nanoparticles with ultra-long circulation and enhanced tumor photothermal therapy. *Biomaterials* **2020**, *231*, 119680.
(10) Yang, W.; Liu, S.; Bai, T.; Keefe, A. J.; Zhang, L.; Ella-Menye, J.-R.; Li, Y.; Jiang, S. Poly(carboxybetaine) nanomaterials enable long circulation and prevent polymer-specific antibody production. *Nano Today* **2014**, *9*, 10−16.
(11) Cui, L.; Lin, Q.; Jin, C. S.; Jiang, W.; Huang, H.; Ding, L.; Muhanna, N.; Irish, J. C.; Wang, F.; Chen, J.; Zheng, G. A PEGylation-Free biomimetic porphyrin banoplatform for personalized cancer theranostics. *ACS Nano* **2015**, *9*, 4484−4495.
(12) Simonsen, J. B. Evaluation of reconstituted high-density lipoprotein (rHDL) as a drug delivery platform − a detailed survey of rHDL particles ranging from biophysical properties to clinical implications. *Nanomedicine* **2016**, *12*, 2161−2179.
(13) Kuai, R.; Li, D.; Chen, Y. E.; Moon, J. J.; Schwendeman, A. High-Density Lipoproteins: Nature's Multifunctional Nanoparticles. *ACS Nano* **2016**, *10*, 3015−3041.
(14) Henrich, S. E.; Thaxton, C. S. An update on synthetic high-density lipoprotein-like nanoparticles for cancer therapy. *Expert Rev. Anticancer Ther.* **2019**, *19*, 515−528.
(15) Pedersbæk, D.; Simonsen, J. B. A systematic review of the biodistribution of biomimetic high-density lipoproteins in mice. *J. Controlled Release* **2020**, *328*, 792−804.
(16) Niora, M.; Pedersbæk, D.; Münter, R.; Weywadt, M. F. d. V.; Farhangibarooji, Y.; Andresen, T. L.; Simonsen, J. B.; Jauffred, L. Head-to-Head Comparison of the Penetration Efficiency of Lipid-Based Nanoparticles into Tumor Spheroids. *ACS Omega* **2020**, *5*, 21162−21171.
(17) Pedersbæk, D.; Jønsson, K.; Madsen, D. V.; Weller, S.; Bohn, A. B.; Andresen, T. L.; Simonsen, J. B. A quantitative ex vivo study of the interactions between reconstituted high-density lipoproteins and human leukocytes. *RSC Adv.* **2020**, *10*, 3884−3894.
(18) Yang, M.; Chen, J.; Cao, W.; Ding, L.; Ng, K. K.; Jin, H.; Zhang, Z.; Zheng, G. Attenuation of nontargeted cell-kill using a high-density lipoprotein-mimicking peptide−phospholipid nanoscaffold. *Nanomedicine* **2011**, *6*, 631−641.
(19) Zhang, Z.; Chen, J.; Ding, L.; Jin, H.; Lovell, J. F.; Corbin, I. R.; Cao, W.; Lo, P. C.; Yang, M.; Tsao, M. S.; Luo, Q.; Zheng, G. HDL-Mimicking Peptide−Lipid Nanoparticles with Improved Tumor Targeting. *Small* **2010**, *6*, 430−437.
(20) Li, D.; Fawaz, M. V.; Morin, E. E.; Ming, R.; Sviridov, D.; Tang, J.; Ackermann, R.; Olsen, K.; Remaley, A. T.; Schwendeman, A. Effect of Synthetic High Density Lipoproteins Modification with Polyethylene Glycol on Pharmacokinetics and Pharmacodynamics. *Mol. Pharmaceutics* **2018**, *15*, 83−96.
(21) Tang, J.; Kuai, R.; Yuan, W.; Drake, L.; Moon, J. J.; Schwendeman, A. Effect of size and pegylation of liposomes and peptide-based synthetic lipoproteins on tumor targeting. *Nanomedicine* **2017**, *13*, 1869−1878.
(22) Murphy, A. J.; Funt, S.; Gorman, D.; Tall, A. R.; Wang, N. Pegylation of high-density lipoprotein decreases plasma clearance and enhances antiatherogenic activity. *Circ. Res.* **2013**, *113*, e1−e9.
(23) Pedersbæk, D.; Kræmer, M. K.; Kempen, P. J.; Ashley, J.; Braesch-Andersen, S.; Andresen, T. L.; Simonsen, J. B. The Composition of Reconstituted High-Density Lipoproteins (rHDL) Dictates the Degree of rHDL Cargo- and Size-Remodeling via Direct Interactions with Endogenous Lipoproteins. *Bioconjugate Chem.* **2019**, *30*, 2634−2646.
(24) Zheng, C. Y.; Ma, G.; Su, Z. Native PAGE eliminates the problem of PEG-SDS interaction in SDS-PAGE and provides an alternative to HPLC in characterization of protein PEGylation. *Electrophoresis* **2007**, *28*, 2801−2807.
(25) Segrest, J. P.; Jones, M. K.; Klon, A. E.; Sheldahl, C. J.; Hellinger, M.; De Loof, H.; Harvey, S. C. A detailed molecular belt model for apolipoprotein A-I in discoidal high density lipoprotein. *J. Biol. Chem.* **1999**, *274*, 31755−31758.
(26) Rajora, M. A.; Zheng, G. Targeting SR-BI for cancer diagnostics, imaging and therapy. *Front. Pharmacol.* **2016**, *7*, 326.
(27) Shen, W.-J.; Azhar, S.; Kraemer, F. B. SR-B1: A Unique Multifunctional Receptor for Cholesterol Influx and Efflux. *Annu. Rev. Physiol.* **2018**, *80*, 95−116.

(28) Liadaki, K. N.; Liu, T.; Xu, S.; Ishida, B. Y.; Duchateaux, P. N.; Krieger, J. P.; Kane, J.; Krieger, M.; Zannis, V. I. Binding of High Density Lipoprotein (HDL) and Discoidal Reconstituted HDL to the HDL Receptor Scavenger Receptor Class B Type I. *J. Biol. Chem.* **2000**, *275*, 21262−21271.
(29) Bell, F. P. Lipid Exchange and Transfer Between Biological Lipid-Protein Structures. *Prog. Lipid Res.* **1978**, *17*, 207−243.
(30) Jonas, A.; Kézdy, K. E.; Williams, M. I.; Rye, K.-A. Lipid transfers between reconstituted high density lipoprotein complexes and low density lipoproteins: Effects of plasma protein factors. *J. Lipid Res.* **1988**, *29*, 1349−1357.
(31) Liang, H. Q.; Rye, K. A.; Barter, P. J. Remodelling of reconstituted high density lipoproteins by lecithin:cholesterol acyltransferase. *J. Lipid Res.* **1996**, *37*, 1962−1979.
(32) Scheetz, L. M.; Yu, M.; Li, D.; Castro, M. G.; Moon, J. J.; Schwendeman, A. Synthetic HDL Nanoparticles Delivering Docetaxel and CpG for Chemoimmunotherapy of Colon Adenocarcinoma. *Int. J. Mol. Sci.* **2020**, *21*, 1777.
(33) Wilhelm, S.; Tavares, A. J.; Dai, Q.; Ohta, S.; Audet, J.; Dvorak, H. F.; Chan, W. C. W. Analysis of nanoparticle delivery to tumours. *Nat. Rev. Mater.* **2016**, *1*, 16014.
(34) Nunes, S. S.; Fernandes, R. S.; Cavalcante, C. H.; da Costa César, I.; Leite, E. A.; Lopes, S. C. A.; Ferretti, A.; Rubello, D.; Townsend, D. M.; de Oliveira, M. C.; Cardoso, V. N.; de Barros, A. L. B. Influence of PEG coating on the biodistribution and tumor accumulation of pH-sensitive liposomes. *Drug Delivery Transl. Res.* **2019**, *9*, 123−130.
(35) Kumar, V.; Mundra, V.; Peng, Y.; Wang, Y.; Tan, C.; Mahato, R. I. Pharmacokinetics and biodistribution of polymeric micelles containing miRNA and small-molecule drug in orthotopic pancreatic tumor-bearing mice. *Theranostics* **2018**, *8*, 4033−4049.
(36) Wang, T.; Subramanian, C.; Yu, M.; White, P. T.; Kuai, R.; Sanchez, J.; Moon, J. J.; Timmermann, B. N.; Schwendeman, A.; Cohen, M. S. Mimetic sHDL nanoparticles: A novel drug-delivery strategy to target triple-negative breast cancer. *Surgery* **2019**, *166*, 1168−1175.
(37) Kuai, R.; Yuan, W.; Son, S.; Nam, J.; Xu, Y.; Fan, Y.; Schwendeman, A.; Moon, J. J. Elimination of established tumors with nanodisc-based combination chemoimmunotherapy. *Sci. Adv.* **2018**, *4*, eaao1736.
(38) Sei, Y. J.; Ahn, J.; Kim, T.; Shin, E.; Santiago-Lopez, A. J.; Jang, S. S.; Jeon, N. L.; Jang, Y. C.; Kim, Y. Detecting the functional complexities between high-density lipoprotein mimetics. *Biomaterials* **2018**, *170*, 58−69.
(39) Oliveira, S.; Cohen, R.; Walsum, M.; van Dongen, G. A.; Elias, S. G.; van Diest, P. J.; Mali, W.; van Bergen en Henegouwen, P. M. A novel method to quantify IRDye800CW fluorescent antibody probes ex vivo in tissue distribution studies. *EJNMMI Res.* **2012**, *2*, 50.
(40) Baković, D.; Valic, Z.; Eterović, D.; Vuković, I.; Obad, A.; Marinović-Terzić, I.; Dujić, Z. Spleen volume and blood flow response to repeated breath-hold apneas. *J. Appl. Physiol.* **2003**, *95*, 1460−1466.
(41) Perez-Medina, C.; Tang, J.; Abdel-Atti, D.; Hogstad, B.; Merad, M.; Fisher, E. A.; Fayad, Z. A.; Lewis, J. S.; Mulder, W. J. M.; Reiner, T. PET Imaging of Tumor-Associated Macrophages with 89Zr-Labeled High-Density Lipoprotein Nanoparticles. *J. Nucl. Med.* **2015**, *56*, 1272−1277.
(42) Yang, H.; Fogo, A. B.; Kon, V. Kidneys: Key modulators of high-density lipoprotein levels and function. *Curr. Opin. Nephrol. Hypertens.* **2016**, *25*, 174−179.
(43) Münter, R.; Kristensen, K.; Pedersbæk, D.; Larsen, J. B.; Simonsen, J. B.; Andresen, T. L. Dissociation of fluorescently labeled lipids from liposomes in biological environments challenges the interpretation of uptake studies. *Nanoscale* **2018**, *10*, 22720−22724.
(44) Zhang, P.; Sun, F.; Liu, S.; Jiang, S. Anti-PEG antibodies in the clinic: Current issues and beyond PEGylation. *J. Controlled Release* **2016**, *244*, 184−193.

https://dx.doi.org/10.1021/acsomega.0c05468
ACS Omega 2021, 6, 871−880